CALIBRATION OF TENSORIAL DAMAGE CONCRETE MATERIAL MODEL WITH CYCLIC COMPRESSION TESTS AND ULTRASOUND MEASUREMENTS

Kim Calonius[1], Alexis Fedoroff[2], Oskari Jessen-Juhler[3], Antti Forsström[3]

[1] Senior Scientist, VTT Technical Research Centre of Finland Ltd., Finland (kim.calonius@vtt.fi)
[2] Senior Scientist, VTT Technical Research Centre of Finland Ltd., Finland
[3] Research Scientist, VTT Technical Research Centre of Finland Ltd., Finland

ABSTRACT

It is well known, that under uniaxial compression, a concrete specimen undergoes very different damage patterns in the loading direction when compared to the damage in the directions orthogonal to loading. Correct modelling of the anisotropic damage evolution in concrete can be described using tensor valued damage and/or plasticity internal variables as opposed to scalar valued variables, as shown in Vilppo et al. (2021). However, the drawback of such models is the calibration of a large number of model parameters. This study investigates the feasibility of using multi-directional ultrasound wave speed measurements in damaged concrete specimens to determine the anisotropic damage state. From the relation between wave speed measurements in different directions and stiffness tensor components, one can deduce the evolution of the stiffness tensor as a function of accumulated inelastic strain in loading direction.

MOTIVATION

In traditional engineering design, it is usually assumed that nuclear power plant reinforced concrete structures respond in a range of quasi-linear stress-strain response to design basis (DB) seismic loads. Hence, in engineering design basis analyses the material model used for reinforced concrete is typically an isotropic material with linear-elastic stress strain response. Recently, there is a growing interest in design extension conditions (DEC), or beyond design basis external hazards. DEC earthquake scenarios, defined by regulators, are significantly more demanding compared to earlier DB scenarios. Fulfilling the DEC criteria requires the use of non-linear stress-strain responses for concrete in structural elements that are critical for lateral load resistance (e.g. shear walls) and a correct modelling of reinforced concrete failure modes in the direction of loading and in the directions perpendicular to loading.

Modelling the correct anisotropic non-linear response of reinforced concrete shear walls under cyclic dynamic loading is a non-trivial task. The conclusion of a recent benchmark exercise on matching simulation responses to shear wall experimental results, NECS, (2016), pinpoints an important scattering of the simulation results. To our understanding, some of the difficulties of correct modelling of concrete behaviour resides in three major topics that need to be addressed: 1) Anisotropic behaviour of damaged concrete, even though virgin concrete may be considered as isotropic. 2) Stiffness degradation and stiffness recovery mechanisms in concrete under complex loading histories. 3) Frictional dissipation due to crack opening and closing in damaged concrete and correct modelling of the hysteresis loops. This study focuses primarily on the anisotropic behavior of damaged concrete. An attempt to understand the anisotropic damage behavior of concrete has been conducted in a derivation of a tensorial elastic-damage model for quasi-brittle materials, Vilppo, et al., (2021). Other concrete modelling work focuses on frictional dissipation aspects, Richard & Ranguneau, (2013).

Material model development is a trial and error process, which aims at finding the most appropriate mathematical description, such that the response of the model matches the response obtained from a number of experimental stress-strain situations. Comprehensive calibration of the model parameters is the key to a later successful use of the model in full scale simulations. The most natural way to calibrate a tensorial damage model is with respect to the evolution of the tangent stiffness tensor as a function of accumulated inelastic strain. From the measurements of ultrasound velocities of P-waves and S-waves in different directions of the damaged concrete specimen, and the relations between ultrasound velocities and stiffness tensor components, Brown, (2001), one gets the necessary calibration data for a tensorial damage model.

UNIAXIAL CYCLIC COMPRESSIVE TESTS ON CUBE SPECIMENS

Three cubic concrete specimens of nominal dimensions 100mm are tested in a uniaxial compressive cyclic displacement driven test using a hydraulic press with hinged loading plate on the top. Figure 1 shows the test setup. For each specimen 6 loading cycles are carried out.
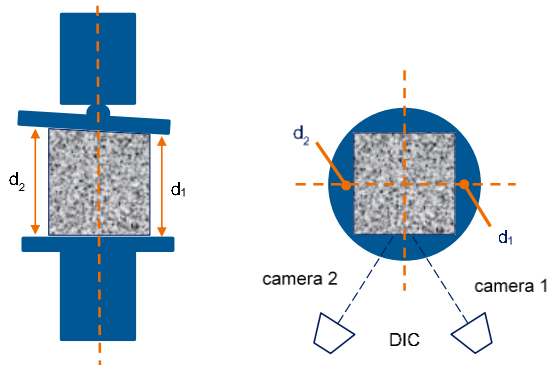
Figure 1. Alignment of displacement transducers and position of cameras (side and top view).

The instrumentation in the tests consists in two displacement transducers placed on each side of the specimen that measure the displacement of points d_1 and d_2 as per Figure 1 between the moving plate and the fixed plate. The average value of d_1 and d_2 divided by the specimen height gives the compressive axial engineering strain of the specimen. The measured force divided by the specimen cross-sectional area gives the engineering compressive stress of the specimen. Stress-strain curves are shown in Figure 2.
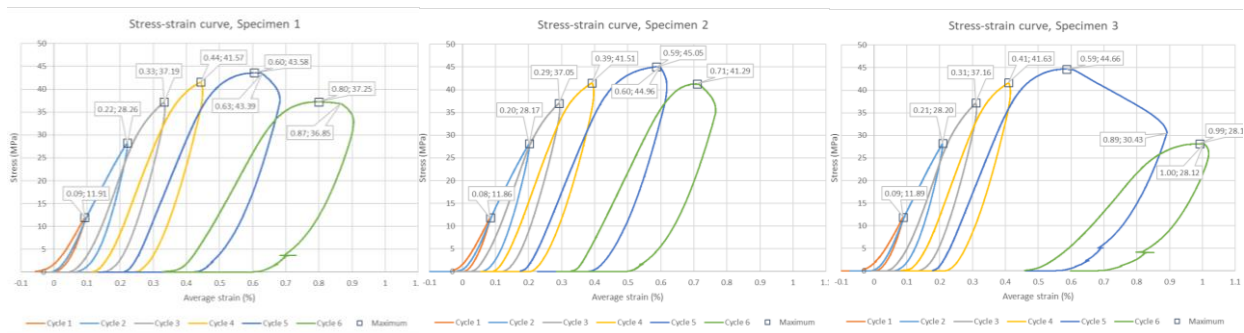
Figure 2. Axial stress-strain curves for three concrete cubic specimens

Table 1 shows some numerical values that can be calculated from the stress-strain data. Maximum loading/unloading stiffness is the maximum value of the slope on the loading/unloading range of the stress-strain cycle. Peak stress denotes the maximum stress recorded during the cycle. Unload stress denotes the

stress value at which the loading direction is reversed. Unload total strain denotes the strain value at which loading direction is reversed, whereas unload plastic strain denotes the residual strain value at the end of a cycle, when all loading is removed.

Table 1. Axial stress-strain curves for three concrete cubic specimens

	cycle	Max loading stiffness	Strain at max loading stiffness	Max unloading stiffness	Strain at max unloading stiffness	Peak stress	Strain at peak stress	Unload stress	Unload total strain	Unload plastic strain
		GPa	%	GPa	%	MPa	%	MPa	%	%
Specimen 1	1	13.9	0.093	26.2	0.093	11.9	0.093	11.9	0.093	0.006
	2	15.4	0.115	37.3	0.222	28.3	0.222	28.3	0.222	0.076
	3	19.6	0.186	35.8	0.335	37.2	0.333	37.2	0.333	0.164
	4	18.9	0.260	34.7	0.449	41.6	0.443	41.6	0.443	0.261
	5	17.7	0.339	30.0	0.683	43.6	0.605	43.4	0.630	0.448
	6	13.4	0.542	25.7	0.905	37.2	0.799	36.9	0.870	0.614
Specimen 2	1	14.3	0.074	28.8	0.084	11.9	0.084	11.9	0.084	0.008
	2	16.5	0.101	36.5	0.202	28.2	0.202	28.2	0.202	0.064
	3	20.1	0.154	38.8	0.294	37.0	0.292	37.0	0.292	0.126
	4	20.0	0.221	37.4	0.397	41.5	0.392	41.5	0.392	0.209
	5	17.6	0.305	33.4	0.618	45.1	0.586	45.0	0.600	0.387
	6	15.6	0.482	28.2	0.766	41.3	0.710	41.3	0.710	0.505
Specimen 3	1	14.4	0.088	28.7	0.088	11.9	0.088	11.9	0.088	0.008
	2	16.2	0.106	40.3	0.209	28.2	0.209	28.2	0.209	0.067
	3	20.3	0.173	39.2	0.312	37.2	0.310	37.2	0.310	0.140
	4	19.9	0.241	36.3	0.415	41.6	0.410	41.6	0.410	0.222
	5	17.9	0.307	20.2	0.892	44.7	0.587	30.4	0.890	0.569
	6	8.5	0.711	18.7	1.019	28.1	0.991	28.1	1.000	0.696

ULTRASOUND MEASUREMENT METHODOLOGY

Ultrasonic measurements are carried out with Proceq pundit ultrasonic device, using the pitch and catch technique with first received signal. The transmitting probe is set on one side of the cube and the receiving probe on the opposite side of the cube. The longitudinal wave probe uses a frequency of 54 kHz and the shear wave probe uses frequency of 40 kHz. Ultrasonic gel is used as a couplant for the longitudinal wave probe. The longitudinal (p) wave probe was calibrated with an acrylic reference bar. The shear (s) wave measurements were calibrated with a known copper material. Figure 3 shows the test setup for longitudinal wave probe.

Figure 3. Ultrasonic measurement equipment

The directions and concrete cube face nomenclature used in the ultrasound measurements are shown in Figure 4.
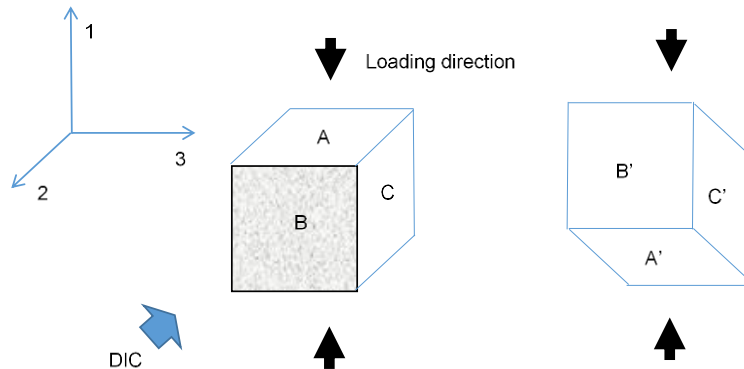
Figure 4. Concrete test cube face nomenclature

The ultrasound measurements are carried out on the concrete cube specimens according to the test matrix shown in Table 2. Such a set of ultrasound measurements is carried out first on a virgin concrete test cube, then at the end of each loading-unloading cycle. The test cube needs to be removed from the hydraulic press to carry out the ultrasound measurements, after which the test cube is carefully replaced in the hydraulic press in the same position.

Table 2. Ultrasound measurement test matrix

wavefront direction	polarization direction	sensor	Signal transmitter side	Signal receiver side	sound velocity v_{ij}
1	1	p	A	A'	v_{11}
1	1	p	A'	A	
2	2	p	B	B'	v_{22}
2	2	p	B'	B	
3	3	p	C	C'	v_{33}
3	3	p	C'	C	
1	2	s − 0°	A	A'	v_{12}
1	2	s − 0°	A'	A	
1	3	s − 90°	A	A'	v_{13}
1	3	s − 90°	A'	A	
2	3	s − 0°	B	B'	v_{23}
2	3	s − 0°	B'	B	
2	1	s − 90°	B	B'	v_{21}
2	1	s − 90°	B'	B	
3	1	s − 0°	C	C'	v_{31}
3	1	s − 0°	C'	C	
3	2	s − 90°	C	C'	v_{32}
3	2	s − 90°	C'	C	

The measurements are done by attaching an ultrasonic transducer onto an ultrasound device, and the sound is propagated from the transmitting to the receiver probe (pitch-catch measurement). In homogeneous isotropic media, the propagation velocity of the p-wave, v_p relates to the density ρ and the p-wave modulus $M = E(1 − v)/(1 − v − 2v^2)$ by the relation $v_p = \sqrt{M/\rho}$. Likewise, in homogeneous isotropic media the

propagation velocity of the s-wave, v_s relates to the shear modulus $G = E/(2 + 2v)$ by the relation $v_s = \sqrt{G/\rho}$. However, damaged concrete is anisotropic, which implies that the relations $v_p = \sqrt{M/\rho}$ and $v_s = \sqrt{G/\rho}$ cannot be used. Following the derivation in Brown, (2001), from the eigensolutions of the Kelvin-Christoffel matrix, one can deduce the relation between soundwave velocities v_{ij} and the stiffness tensor components E_{mnpq}, where the indexes i and j refer, respectively, to the wavefront and polarization directions and the indexes m, n, p and q refer to the stiffness tensor components. Hence, for p-wave measurements in the principal directions one gets:

$$E_{1111} = \rho v_{11}{}^2, \qquad E_{2222} = \rho v_{22}{}^2, \qquad E_{3333} = \rho v_{33}{}^2 \qquad (1)$$

For s-wave measurements in the principal directions one gets:

$$\begin{aligned}
E_{2323} &= \rho v_{23}{}^2, & E_{3131} &= \rho v_{31}{}^2, & E_{1212} &= \rho v_{12}{}^2, \\
E_{3232} &= \rho v_{32}{}^2, & E_{1313} &= \rho v_{13}{}^2, & E_{2121} &= \rho v_{21}{}^2 .
\end{aligned} \qquad (2)$$

Notice, that in the measurements it was recorded that $v_{12} \neq v_{21}$, $v_{31} \neq v_{13}$ and $v_{23} \neq v_{31}$ in a general case for damaged concrete, which implies that some of the stiffness tensor symmetry properties are lost. Ultrasound measurements in the three principal directions yields only 6 out of the 9 stiffness tensor components for orthotropic media. For the determination of the remaining stiffness tensor components E_{2233}, E_{3311} and E_{1122}, one has to consider the diagonal directions: direction 4 corresponding to $(0,1,1)$ in global coordinates, direction 5 corresponding to $(1,0,1)$ in global coordinates and direction 6 corresponding to $(1,1,0)$ in global coordinates. Notice, that for the wavefront direction 4, the polarization direction is quasi-longditudinal, $(0, \cos \gamma_4 , \sin \gamma_4) \approx (0,1,1)$ if we assume that $E_{2222} \approx E_{3333}$. Likewise, for the wavefront direction 5, the polarization direction is quasi-longditudinal, $(\cos \gamma_5 , 0, \sin \gamma_5) \approx (1,0,1)$, if we assume that $E_{1111} \approx E_{3333}$. Finally, for the wavefront direction 6, the polarization direction is quasi-longditudinal, $(\cos \gamma_6 , \sin \gamma_6 , 0) \approx (1,1,0)$ if we assume that $E_{1111} \approx E_{2222}$. Hence, by taking measurements with the P-wave sensor along the diagonal directions 4, 5 and 6, one can determine the remaining unknown stiffness tensor components as per Equation 3:

$$\begin{aligned}
E_{2233} &= \rho \left(\frac{1}{2}\sqrt{(4v_{44}{}^2 - v_{22}{}^2 - 2v_{23}{}^2 - v_{33}{}^2)^2 - (v_{22}{}^2 - v_{33}{}^2)^2} - v_{23}{}^2 \right), \\
E_{3311} &= \rho \left(\frac{1}{2}\sqrt{(4v_{55}{}^2 - v_{33}{}^2 - 2v_{31}{}^2 - v_{11}{}^2)^2 - (v_{33}{}^2 - v_{11}{}^2)^2} - v_{31}{}^2 \right), \\
E_{1122} &= \rho \left(\frac{1}{2}\sqrt{(4v_{66}{}^2 - v_{11}{}^2 - 2v_{12}{}^2 - v_{22}{}^2)^2 - (v_{11}{}^2 - v_{22}{}^2)^2} - v_{12}{}^2 \right).
\end{aligned} \qquad (3)$$

The eigenmode directions of the Kelvin-Christoffel matrix are given by Equation 4.

$$\begin{aligned}
\tan \gamma_4 &= \left(E_{2222} - E_{3333} + \sqrt{(E_{2222} - E_{3333})^2 + 4(E_{2233} + E_{2323})^2} \right) / \left(2(E_{2233} + E_{2323}) \right), \\
\tan \gamma_5 &= \left(E_{3333} - E_{1111} + \sqrt{(E_{3333} - E_{1111})^2 + 4(E_{3311} + E_{3131})^2} \right) / \left(2(E_{3311} + E_{3131}) \right), \\
\tan \gamma_6 &= \left(E_{1111} - E_{2222} + \sqrt{(E_{1111} - E_{2222})^2 + 4(E_{1122} + E_{1212})^2} \right) / \left(2(E_{1122} + E_{1212}) \right).
\end{aligned} \qquad (4)$$

Ultrasound measurements along diagonal directions require chamfered cubes, as shown in Figure 5. However, due to budgetary constraints, it was not possible to carry out tests on chamfered cubes during the 2021 test campaign, and therefore in this study experimental ultrasound measurement data is presented only on 6 stiffness tensor components out of 9.
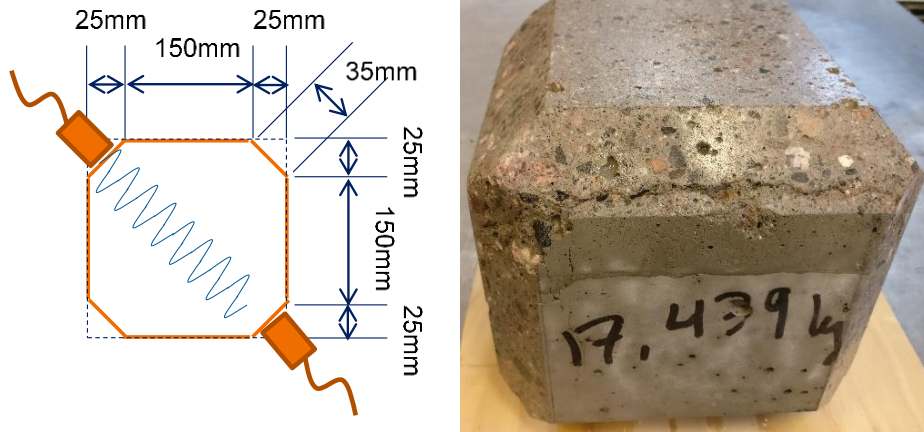
Figure 5. Example of a chamfered concrete cube specimen.

ULTRASOUND MEASUREMENT TEST RESULTS

Ultrasound measurement test results are shown in Figure 6 for longitudinal wave velocities, and in Figures 7 and 8 for shear wave velocities. Each data point represents the average of two readings: in direction 1, the average is for the sound velocity measurement with transmitter probe placed on face A and receiver probe on A' and sound velocity measurement with transmitter probe placed on face A' and receiver probe on A. Likewise, in direction 2, the average is for the sound velocity with transmitter probe placed on face B and receiver probe on B' and sound velocity with transmitter probe placed on face B' and receiver probe on B. For direction 3, the average is for the sound velocity with transmitter probe placed on face C and receiver probe on C' and sound velocity with transmitter probe placed on face C' and receiver probe on C.

The data points are grouped together for measurements from all specimens (Specimen 1, Specimen 2 and Specimen 3). Dashed lines show exponential fit through the data points.
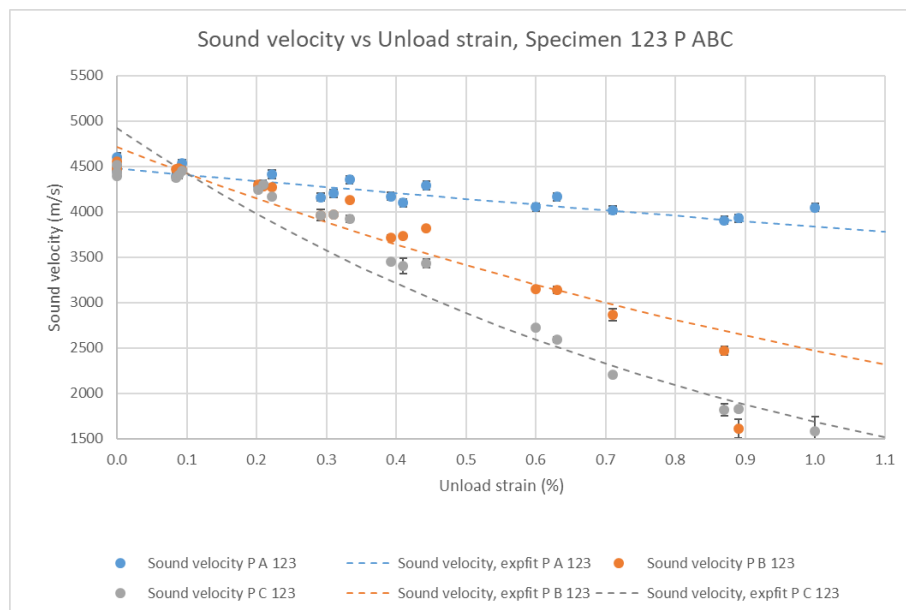
Figure 6. P-wave velocity vs. unload total strain plot
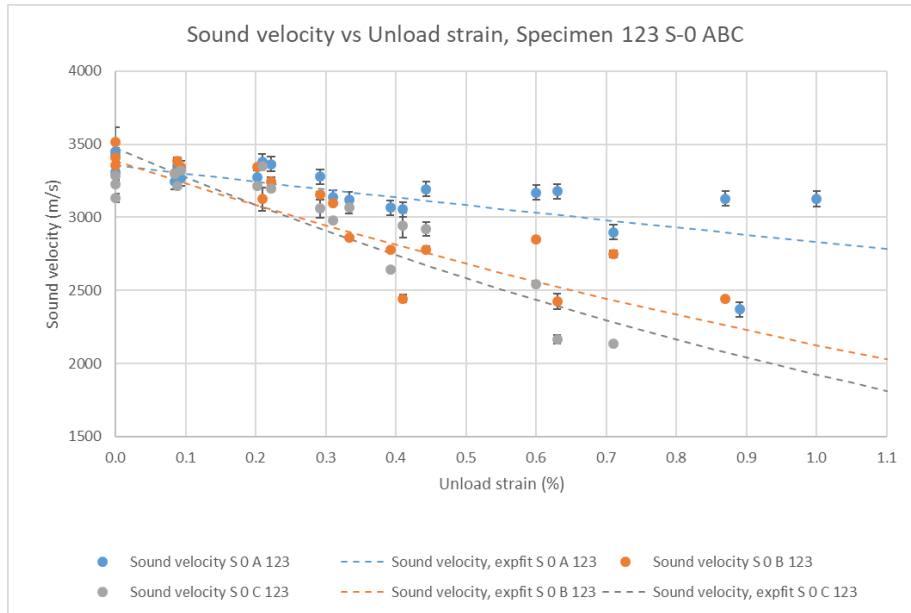
Figure 7. S-wave velocity at 0° polarization vs. unload total strain plot
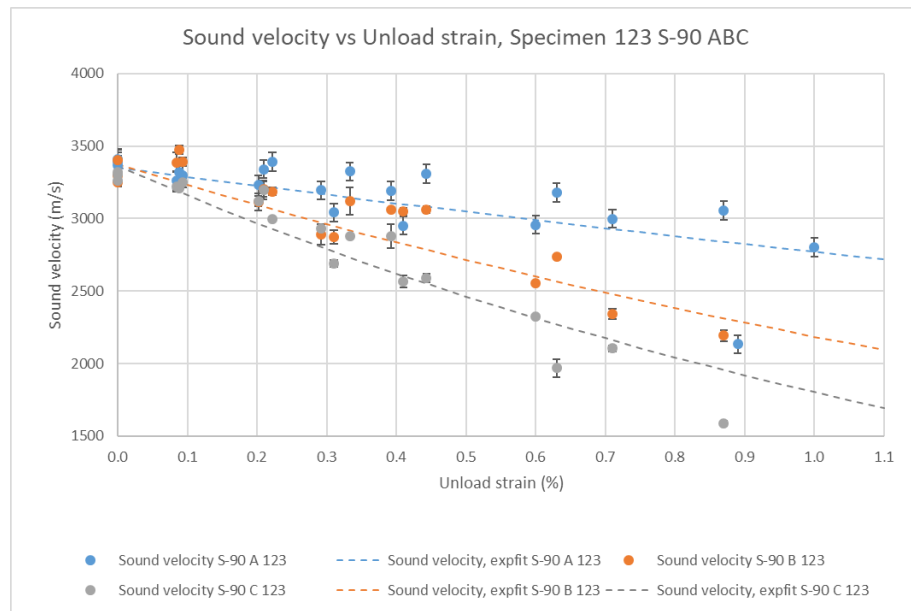
Figure 8. S-wave velocity at 90° polarization vs. unload total strain plot

From ultrasound wave speed measurements 6 out of 9 stiffness tensor components for orthotropic media are computed. Notice, that the break of symmetry properties of the stiffness tensor $E_{ijij} \neq E_{jiji}$ results for three (3) extra components shown in Table 3. Figure 9 shows the evolution of stiffness tensor components E_{1111}, E_{2222} and E_{3333}. Figure 10 shows the evolution of stiffness tensor components E_{2323}, E_{3131} and E_{1212} as well as E_{3232}, E_{1313} and E_{2121}. The fit parameters in Table 3 are computed for Y_i data being the stiffness value in GPa and X_i data being the total unload axial strain in percent. Likewise, the plots in Figures 9 and 10 are plotted against the total unload axial strain on the horizontal axis. It can be argued, that using axial inelastic residual strain values instead of total strain values is a more appropriate way to describe a measure of axial damage, however.

Table 3. Fit parameters for exponential ($y = a\,e^{bx}$) and Gauss functions ($y = a\,e^{-\left(\frac{x-b}{c}\right)^2}$)

tensor	E_{1111}	E_{2222}	E_{3333}	E_{1212}	E_{2323}	E_{3131}	E_{1313}	E_{2121}	E_{3232}
Fit type	exp	Gauss	Gauss	exp	exp	exp	exp	exp	exp
coef a	45.68	46.64	45.63	25.57	27.02	26.57	25.99	26.91	26.35
coef b	-0.2824	-0.0493	-0.0185	-0.1727	-0.7502	-1.049	-0.3106	-0.8255	-1.27
coef c	N/A	0.7696	0.632	N/A	N/A	N/A	N/A	N/A	N/A
R^2	0.8114	0.9781	0.9902	0.5738	0.8476	0.7752	0.6603	0.8369	0.9141
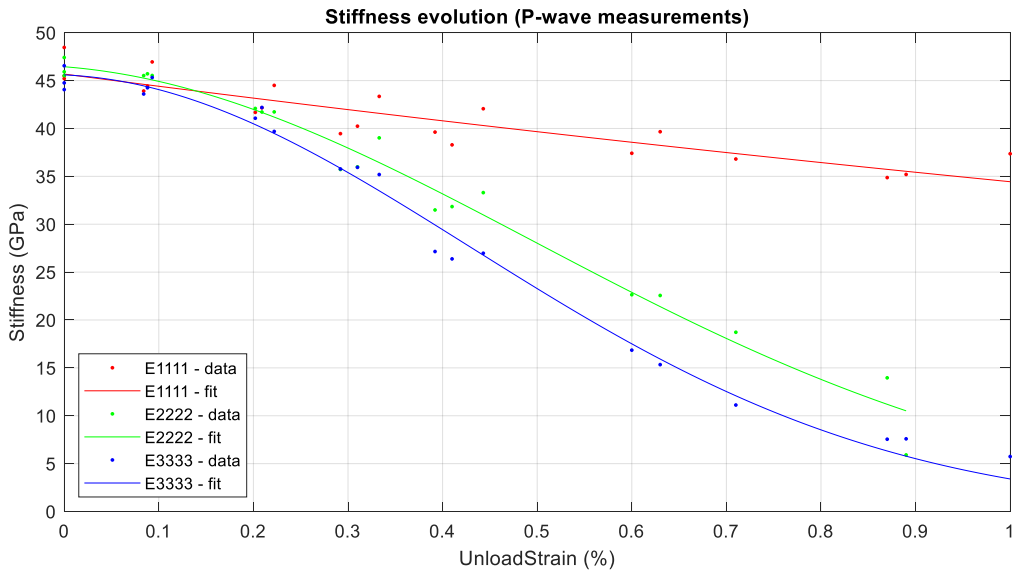
Figure 9. Stiffness evolution computed from P-wave measurements plotted against total unload strain
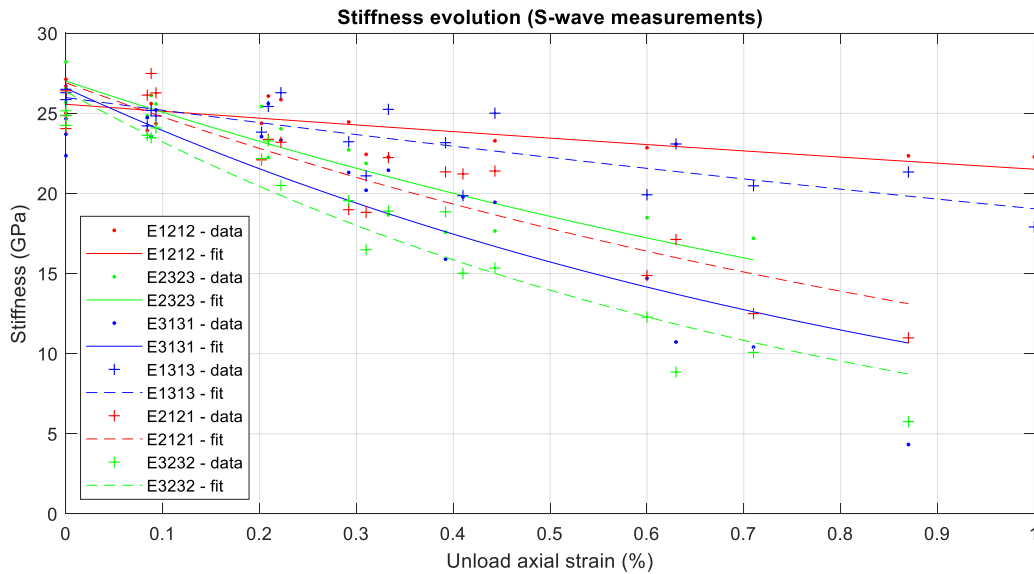
Figure 10. Stiffness evolution computed from S-wave measurements plotted against total unload strain

COMPARISON OF ULTRASOUND AND MECHANICAL MEASUREMENTS

From the mechanical displacement measurements one can compute the maximum loading and unloading stiffness values, as shown in Table 1. Although according to the continuum damage-plasticity theory the reload and unload stiffness values should be equal, for concrete a hysteresis behaviour is observed (Figure 11). It is of common practice in damage-plasticity theory that the total strain is decomposed as a sum of inelastic residual strains and damage-elastic strains. The inelastic residual strain can be considered as a measure of the amount of axial damage accumulated at the material point.
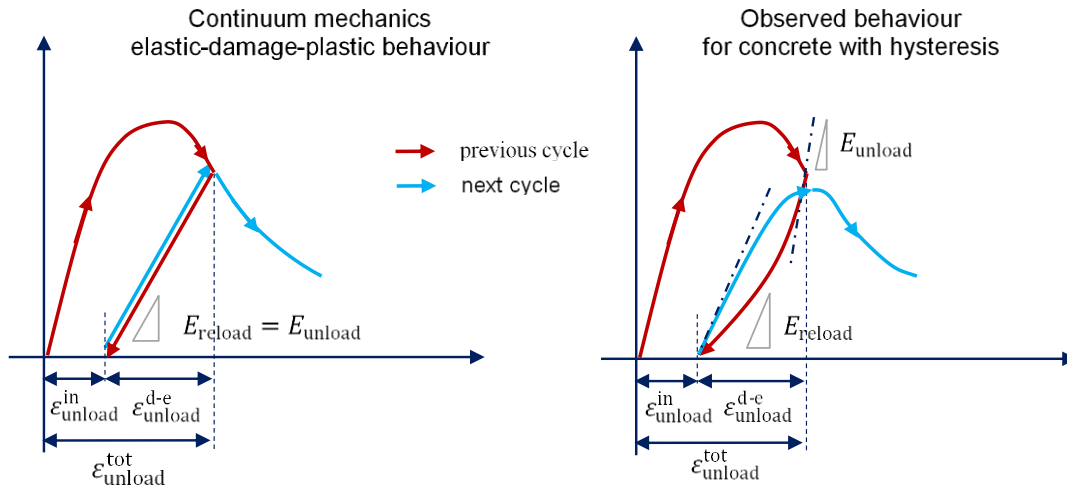
Figure 11. Schematic representation of loading-unloading cycles

Figure 12 shows comparative plots of the stiffness evolution of component E_{1111}, computed both from the ultrasound wave speed measurements and from the mechanical displacement measurements. It can be observed, that when plotted against inelastic residual strains, the stiffness values predicted by the exponential fit from ultrasound measurements (black line) are exactly the same than the ones predicted by the exponential fit for unload stiffness values (red dashed line) for virgin concrete. However, for damaged concrete, the stiffness values from ultrasound measurements overestimate the unload stiffness values from mechanical measurement. Notice, that in the computation of the exponential fits for unload and reload stiffness, the first data points are considered as outliers. These outlier points correspond to "non-stabilized[1]" measurement values of the secant stiffness.

The reason why the stiffness evolution calculated from ultrasound measurements and mechanical measurements differ for damaged concrete remains to be elucidated. One possible explanation is that both the unload and reload stiffness values are computed from a test specimen under a stress state, whereas the ultrasound measurements are carried out on a test specimen in a stress-free state, such that most of the micro-cracks are closed. It can also be argued that actually the stiffness values computed from soundwave velocities in a stress-free state are, actually, much more appropriate measures of stiffness than the ones computed from a specimen under stress.

---

[1] In concrete secant stiffness determination test standards, the stabilized value of secant stiffness corresponds to a secant slope measurement from the stress-strain curve after a sufficient number of loading-unloading cycles.
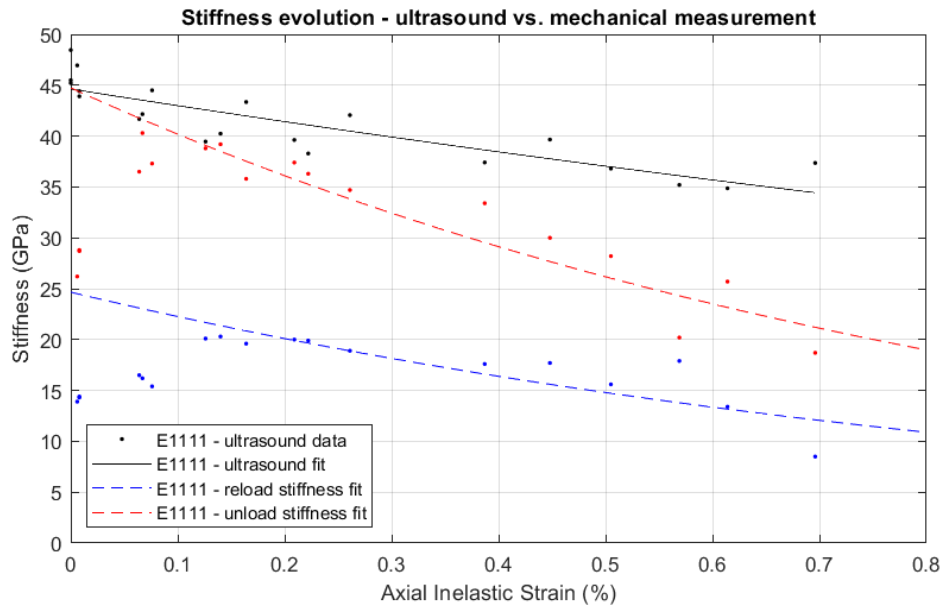
Figure 12. Stiffness evolution of component E_{1111}, ultrasound vs. mechanical measurement

SUMMARY AND CONCLUSIONS

In this research, cyclic compression tests were carried out on concrete specimens in order to figure out how the stiffness properties of damaged concrete evolve with damage. The measure of concrete damage chosen in this study is the axial inelastic residual strain at unloading. The measure of stiffness is carried out in two ways. First, the stiffness tensor components are calculated from ultrasound wave speed measurements in three principal directions of the concrete specimen and with three different polarization directions. In addition, axial unload and reload stiffness values are measured from the slope of the stress-strain curve during the loading phase of each cycle and the unloading phase of each cycle. Comparison of the axial stiffness component values from ultrasound and mechanical measurement shows that for damaged concrete stiffness computed from ultrasound measurement gives higher values. The purpose of this entire study is primarily to serve as a proof of feasibility of damaged concrete stiffness determination from ultrasound measurements. In subsequent studies, planned to be realized in 2022, more thorough ultrasound measurements will be performed both in the principal directions of the test specimen and in the diagonal directions.

REFERENCES

Brown, R. J., (2001). "Relationships between the velocities and the elastic constants of an anisotropic solid possessing orthorombic symmetry", s.l.: *CREWES project*.

NECS, (2016). CASH Benchmark on the beyond design seismic capacity of reinforced concrete shear walls, PRESENTATION OF THE CASH BENCHMARK PHASE 1 B, Paris: NECS civil engineering expertise an consultancy.

Richard, B. & Ranguneau, F., (2013). "Continuum damage mechanics based model for quasi brittle materials subjected to cyclic loadings: Formulation, numerical implementation and applications." *Engineering Fracture Mechanics*, p. 383–406.

Vilppo, J., Kouhia, R., Hartikainen, J., Kolari, K., Fedoroff, A. and Calonius, K. (2021). "Anisotropic damage model for concrete and other quasi-brittle materials." *International Journal of Solids and Structures*, Volume 225.